MOLECULAR ELECTRONICS

Ferroelectric self-assembled molecular materials showing both rectifying and switchable conductivity

Andrey V. Gorbunov,[1] Miguel Garcia Iglesias,[2] Julia Guilleme,[3] Tim D. Cornelissen,[4] W. S. Christian Roelofs,[1] Tomas Torres,[3,5] David González-Rodríguez,[3] E. W. Meijer,[2] Martijn Kemerink[1,4]*

Copyright © 2017 The Authors, some rights reserved; exclusive licensee American Association for the Advancement of Science. No claim to original U.S. Government Works. Distributed under a Creative Commons Attribution NonCommercial License 4.0 (CC BY-NC).

Advanced molecular materials that combine two or more physical properties are typically constructed by combining different molecules, each being responsible for one of the properties required. Ideally, single molecules could take care of this combined functionality, provided they are self-assembled correctly and endowed with different functional subunits whose strong electronic coupling may lead to the emergence of unprecedented and exciting properties. We present a class of disc-like semiconducting organic molecules that are functionalized with strong dipolar side groups. Supramolecular organization of these materials provides long-range polar order that supports collective ferroelectric behavior of the side groups as well as charge transport through the stacked semiconducting cores. The ferroelectric polarization in these supramolecular polymers is found to couple to the charge transport and leads to a bulk conductivity that is both switchable and rectifying. An intuitive model is developed and found to quantitatively reproduce the experimental observations. In a larger perspective, these results highlight the possibility of modulating material properties using the large electric fields associated with ferroelectric polarization.

INTRODUCTION

Both processable and highly organized semiconducting molecules, which exhibit intriguing charge-transfer properties (*1*), and self-assembled (liquid) crystals, which qualify as organic ferroelectric materials (*2*–*4*), have been reported. However, the combination of these properties in a single compound has so far remained elusive. For combining semiconductivity and ferroelectricity, it will be necessary to spatially separate the molecular dipoles, which need motional freedom to be aligned, from the stacked π-conjugated fragments. At the same time, the strongest coupling between the two functionalities is anticipated when their separation is minimal. Therefore, we designed special disc-shaped molecules where the rigid core is based on well-known π-conjugated units, such as perylene bisimides (PBI) and (sub)phthalocyanines (Pc and SubPc). The flexible side groups, which are normally used for solubility and intramolecular phase separation, are modified to have either an amide or an oligovinylidene difluoride (oVDF) unit, both known to form strong polar arrangements in a cooperative way (Fig. 1). When properly organized in the solid state, columnar-like ordered architectures result, enabling efficient charge transport (*1*, *5*, *6*) and ferroelectric switching. The rationale for this design is that the ferroelectric polarization will establish an asymmetric potential that can be expected to couple to the bulk conductivity as it leads to a nonequivalence of current flow along and against the polarization direction, giving rise to conductivity that is directional (rectifying) and switchable.

Such behavior, so far not observed, could be considered the all-electrical equivalent of the bulk photovoltaic effect, that is, the rectification of light that is observed in piezo- and ferroelectric crystals, typically inorganic perovskites (*7*). Whereas inorganic crystals have to be prepared by high-temperature vacuum deposition techniques, the organic materials presented here can be used directly after a simple combination of solution processing and field annealing. Likewise, the modulation of the bulk conductivity of a single compound differs fundamentally from the modulation of an injection barrier that gives rise to switchable currents in phase-separated blends of semiconducting and ferroelectric polymers (*8*–*11*), in ferroelectric Schottky diodes (*12*, *13*), and, recently, in a single organic compound (*14*).

RESULTS AND DISCUSSION

To realize the above, we synthesized three materials as indicated in Fig. 1. Details about the chemical synthesis and characterization of these molecules can be found in section S1 and in studies of Guilleme *et al.* (*15*) and García-Iglesias *et al.* (*16*). The SubPc material forms a hexagonal liquid crystalline phase at room temperature and over a broad temperature range (up to 250°C), where hydrogen bonding between the amide groups stabilizes the quasi-1D (one-dimensional) columnar arrangement (section S1) (*15*, *17*). Stable homeotropic alignment was confirmed by polarization optical microscopy (POM; section S2). In this arrangement, the amide groups are known to form collective macrodipoles that lead to true ferroelectric behavior (*4*, *18*, *19*). The quasi-static polarization loop at T = 130° to 135°C for the SubPc material is shown in Fig. 2A, and is obtained by integrating the current associated with polarization reversal after subtraction of the leakage current, as described in Materials and Methods. The polarization switches direction when the externally applied electric field passes the coercive field. The remnant polarization of ~0.13 μC/cm^2 is the polarization that remains at zero electric field. The polarization switching is thought to be the result of rotation of the amide group around the C-N bond attaching them to the SubPc core. This polarization is about an order of magnitude less than that observed by Gorbunov *et al.* (*4*) and Fitié *et al.* (*18*, *19*) for the benzene-1,3,5-tricarboxamide material, which reflects the reduced volume density of amide groups and likely a lesser orientational freedom due to different substitution

[1]Department of Applied Physics, Eindhoven University of Technology, P.O. Box 513, 5600 MB Eindhoven, Netherlands. [2]Institute of Complex Molecular Systems, Laboratory of Macromolecular and Organic Chemistry, Eindhoven University of Technology, 5600 MB Eindhoven, Netherlands. [3]Departamento de Química Orgánica (C-I), Facultad de Ciencias, Universidad Autónoma de Madrid, Cantoblanco, 28049 Madrid, Spain. [4]Complex Materials and Devices, Department of Physics, Chemistry and Biology (IFM), Linköping University, 58183 Linköping, Sweden. [5]IMDEA Nanociencia, c/ Faraday 9, 28049 Madrid, Spain.
*Corresponding author. Email: martijn.kemerink@liu.se

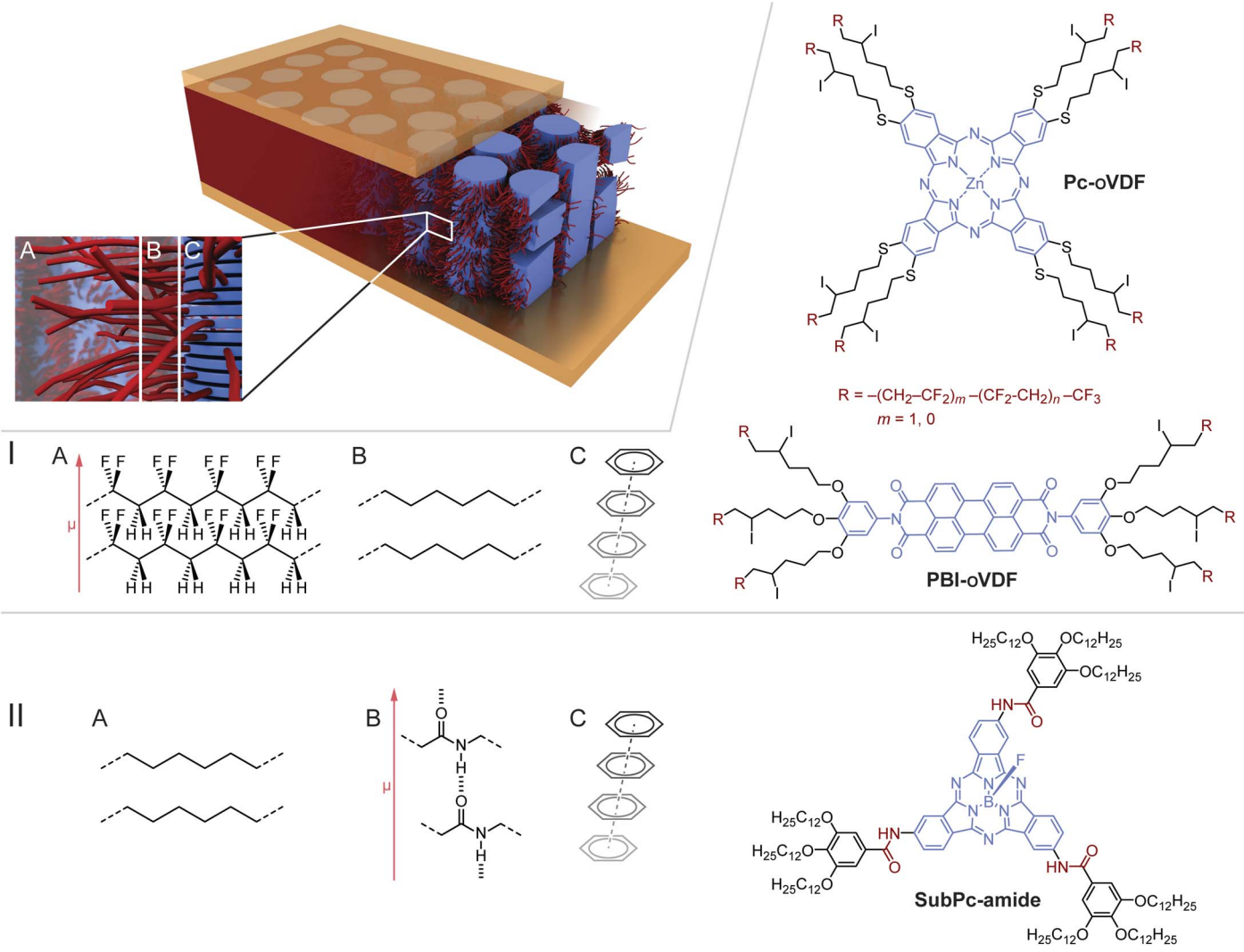

Fig. 1. A cartoon of the devices studied and the chemical structure of the investigated oFESC compounds and their supramolecular organization. Semiconducting cores are shown in blue, and dipolar side groups are shown in red. (I) Structures of PBI-oVDF and Pc-oVDF. (II) Structure of SubPc-amide. For details of the synthesis and characterization, see the Supplementary Materials.

patterns. The latter is known to critically affect the ferroelectric properties of polar molecular materials (*20*).

Current-voltage curves measured on the same organic ferroelectric semiconductor (oFESC) device are shown in Fig. 2B. To minimize spurious currents due to polarization reversal, these are measured at much lower sweep rates than the corresponding polarization loops. At low voltages, the oFESC diodes show a strong rectifying behavior, with a rectification ratio of about an order of magnitude. In this respect, the behavior of our oFESC diodes is reminiscent of the $BiFeO_3$ (BFO) diodes reported by Choi *et al.* (*21*). However, poling our oFESC diodes in reverse direction gives rise to a current that is large in the forward direction, whereas in the BFO-based devices directions of poling and the highest current are parallel. The latter behavior is characteristic of injection barrier modulation, as will be discussed in more detail below (*13*). In stark contrast, the remarkable and unprecedented hysteresis behavior in the current-voltage (jV) loop, indicated by the arrows in Fig. 2, is shown to result from a bulk conductivity modulation. Passing through zero toward positive bias, that is, with negative polarization remaining from the previously negative bias, the device is in a low-resistance state. When reaching biases where the polarization starts to reverse, that is, the coercive field (vertical dotted lines), a region of negative differential resistance is reached and the device enters a high-resistance state. The same happens, *mutatis mutandis* at negative bias.

Qualitatively identical behavior was found in oFESC diodes based on two materials with totally different polar side groups, namely, oVDF chains, as shown in Fig. 3. Infrared spectroscopy of both the PBI-oVDF and Pc-oVDF materials shows the appearance of the ferroelectric β-phase of the oVDF tail, in line with the polar ordering required (*16*). The hysteretic polarization behavior observed in Fig. 3 (A and B) is characteristic of ferroelectric materials. The quantitative variation between the two materials in coercive field and especially remnant polarization is attributed to the evident differences in molecular structure and uncertainty associated with measuring polarization in the presence of a switchable conductance (section S2). Moreover, some fraction of the active material in the oFESC diodes may be in a more disordered state, which does not contribute (or contributes only minimally) to

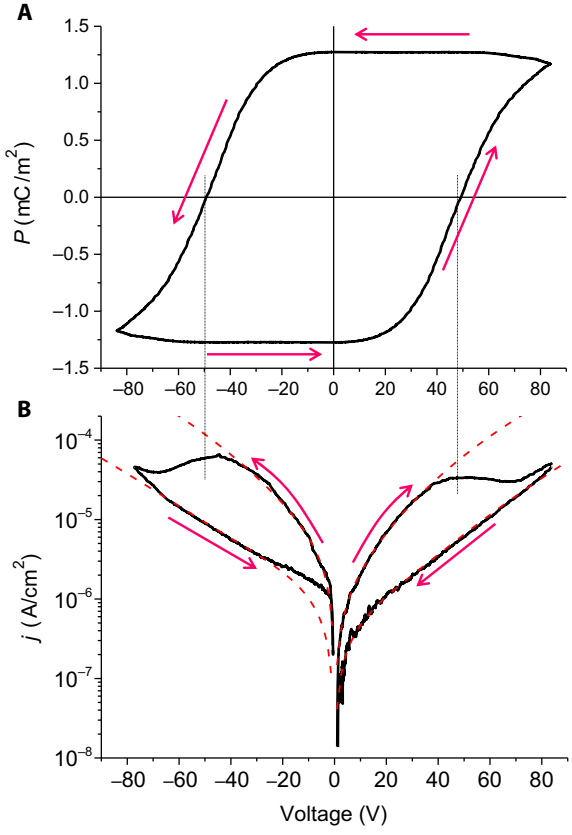

Fig. 2. Simultaneous switching of polarization and conductivity in SubPc-amide. Ferroelectric polarization (**A**) and current (**B**) versus applied bias for a Au/SubPc-amide/Au diode. Polarization and current are separate measurements on the same device. Thin dotted lines indicate the coercive voltage; red dashed lines are fits to a sum of ohmic (Eq. 1) and SCLC (Eq. 2) contributions, showing that conductivity is bulk-limited. Arrows indicate loop sense. Device film thickness L = 1 μm, T = 130° to 135°C.

ferroelectric switching and/or charge transport. The corresponding jV curves in Fig. 3 (C and D) show the same switchable rectification as the SubPc-amide material, which implies that the observed behavior is not a property of a particular molecule but is related to the common molecular design of having a cooperative ordering of the polar side chains in close contact with the stacked semiconducting core.

For actual application in future memory devices, it is important that the rectification can be not only switched and read out once but also done multiple times. Although we did not explicitly investigate the cycling endurance of our devices, we did not observe any signs of switching fatigue during our measurements. In fact, because of improved molecular stacking, the switching curves tend to improve with continuous cycling of one to several hours' duration, corresponding to several thousands of full switching events. Degradation typically occurs stochastically by abrupt shorting, which is not related to the organic material but to the filament formation from the metal contacts (*22–25*).

The correlation between polarization reversal and the change in conductivity strongly suggests a causal relation, as was intended in the molecular design. To substantiate this, the retention of the polarization and conductivity states was investigated. Figure 4 shows that polarization and on-current are lost at essentially the same rate, which leads to the important conclusion that conductivity is directly coupled to polarization state. The retention time on the order of minutes is comparable to previously published molecular ferroelectrics (*19*). We should stress that poor retention is not a fundamental property of this class of ferroelectrics and that minor changes in the molecular structure (*26*) or operational conditions (*27*) can increase the retention time to hours or even months. Moreover, a short retention time does not imply that the material is not a proper ferroelectric (*4*); instead, for the present materials, it likely results from structural disorder and a relatively small energy barrier between the polarization states of single domains (*26*, *27*).

The observed sense of the jV hysteresis loop is opposite to what is found in diodes based on blends of ferroelectric and semiconducting polymers (*8*, *9*). The hysteresis behavior of the latter is well understood to result from a modulation of the charge injection barrier at the metal-semiconductor interface by the ferroelectric polarization (*10*, *11*). The loop sense for these blend devices can be generalized to all devices, where a field-driven redistribution of charge gives rise to a reduction in effective injection barrier height (*13*, *14*) and/or an increase in bulk conductivity, and hence to an increase in current (*28*). For example, in light-emitting electrochemical cells, the redistribution of ions modulates the injection barrier and enables dynamic doping of the semiconductor component (*29*). Both effects lead to a current that increases with time and bias when sweeping from negative to positive bias, opposite to what is observed here. Conventional bipolar resistive switching devices are characterized by on and off states that, at low bias, are off at both polarities (*22–25*, *30*, *31*). In view of the proposed underlying mechanism, the field-driven formation and interruption of conducting filaments, such behavior is logical. The fact that in our oFESC devices the on and off states are exchanged when the polarity of the probe bias is changed excludes filament formation as a possible explanation for our results. Also, the model by Blom *et al.* (*12*) relies on the modulation of an injection barrier, which we can exclude based on the loop sense. This model essentially explains the current modulation as a change in the built-in voltage. As the latter cannot be larger than the bandgap of a few volts, this and similar models can be ruled out, as the current modulation in Fig. 2 would correspond to much larger voltage shifts of a few tens of volts.

The jV curves of all devices presented here can be described by either a simple ohmic conductivity

$$j = \sigma V/L \tag{1}$$

or a space charge limited conductivity (SCLC)

$$j = \frac{9}{8}\varepsilon_0\varepsilon_r\mu_0\frac{V^2}{L^3}\exp(0.891\gamma\sqrt{V/L}) \tag{2}$$

or a sum thereof. Here, V is the applied voltage, L is the layer thickness, σ is the conductivity, $\varepsilon_0\varepsilon_r$ is the dielectric constant of the active layer, μ_0 is the zero-field mobility, and γ is a phenomenological parameter that quantifies the mobility enhancement by the applied electric field. The dashed lines in Figs. 2 and 3 are fits to the jV curves by the sum of Eqs. 1 and 2 (see section S3 for further details). The parameters describing the SCLC behavior (Eq. 2), where these could be determined (SubPc-amide and Pc-oVDF), are in the range expected for this type of small organic molecular semiconductor.

Because both Eqs. 1 and 2 describe currents that are limited by the material bulk, as opposed to those limited by injection or interface barriers associated with the Au contacts, the analysis of the jV curves

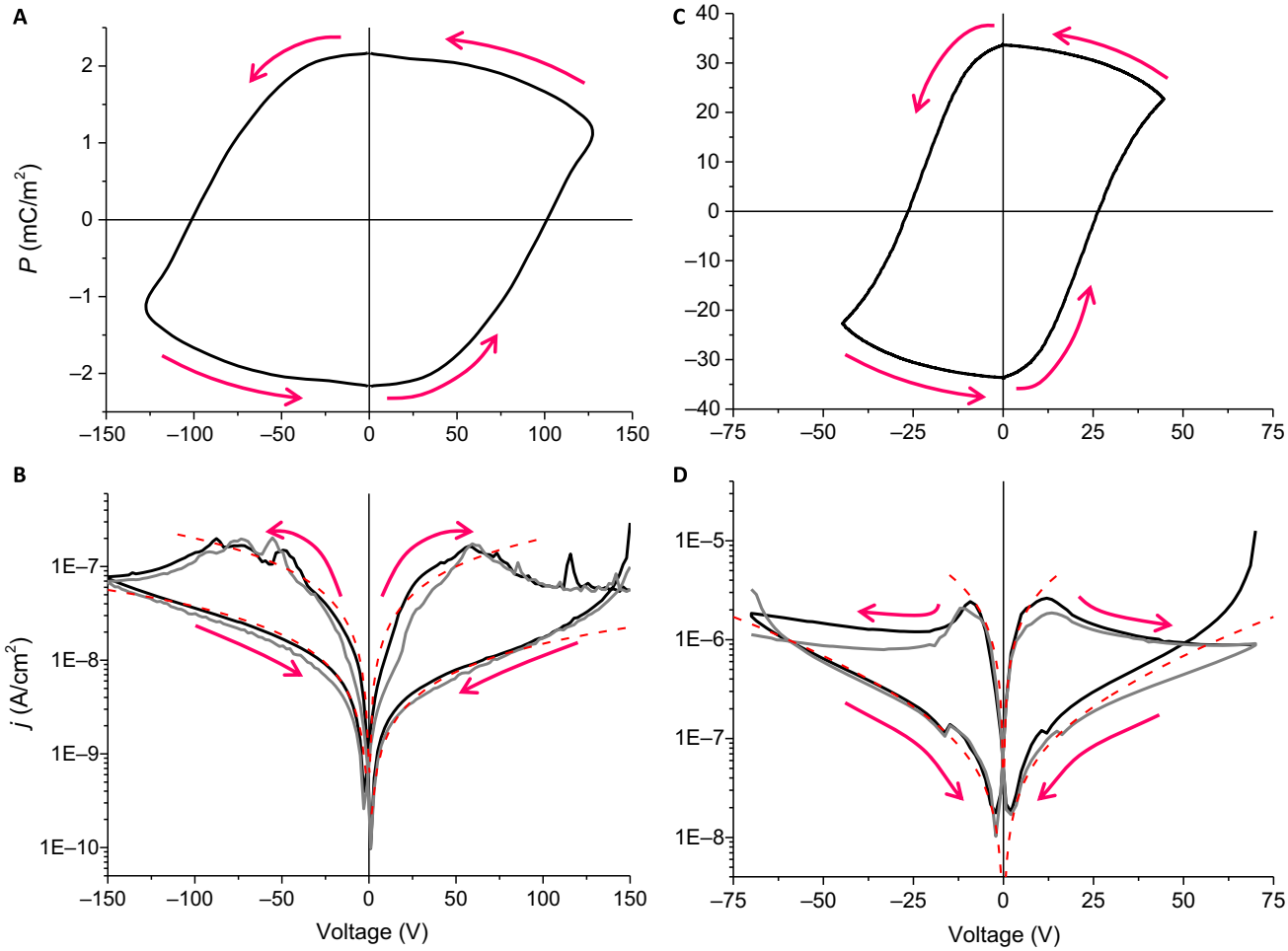

Fig. 3. Simultaneous switching of polarization and conductivity in PBI-oVDF and Pc-oVDF. Ferroelectric polarization (**A** and **C**) and current (**B** and **D**) versus bias for oFESC diodes based on PBI-oVDF (A and B) and Pc-oVDF (C and D). Polarization and current are separate measurements on the same device. Black and gray lines indicate different measurements; red dashed lines are fits consisting of ohmic (Eq. 1) and SCLC (Eq. 2) contributions. Arrows indicate loop sense. (A and B) L = 0.8 μm, T = 55° to 60°C. (C and D) L = 1 μm, T = 40° to 45°C. For jV curves on linear scale, see fig. S15.

leads to the conclusion that the conductivity of our diodes is limited by the bulk in the oFESC diodes. Hence, the bulk conductivity is modulated by the direction and degree of ferroelectric polarization.

To rationalize the above observations, we developed a simple model that captures the essence of charges moving by thermally activated tunneling—hopping—in our systems. In molecular semiconductors, the energies associated with the geometrical reorganization of the initial and final site (molecule) upon charge motion are significant (*1*). The simplest way to account for these polaronic effects on charge motion is by using Marcus hopping rates, which describe the hopping process as a thermally activated motion in a parabolic potential characterized by the reorganization energy λ. The key ingredient of our model is that the proximity of the aligned molecular dipoles to the conjugated molecular core on which the charge sits gives rise to a significant anharmonic and asymmetric contribution to the net potential felt by the moving charge. This potential is calculated in Fig. 5A using numbers that are representative of SubPc. Full details and parameters are given in Materials and Methods and section S5. Adding this asymmetric potential to the harmonic Marcus potential leads, at nonzero field, to a nonequivalence of charge motion along and against the polarization direction, as illustrated in Fig. 5 (B and D). Flipping polarization direction inverts the asymmetric potential and concomitantly the directions of easy and hard charge motion.

Implementing the above process in a transport model that accounts for the complicated percolation system formed by many finite quasi-1D chains in parallel and in series is beyond the scope of this work. We therefore use a two-site hopping model with periodic boundary conditions, which describes the field-dependent hopping between two sites separated by a distance Δz and energy difference ΔE_0 (Fig. 5, B and D). This system represents the critical, that is, rate-limiting, step in the full percolating network. Solving this system for polarization parallel and antiparallel to the field gives the on/off ratio, defined as $j_{\text{parallel}}/j_{\text{antiparallel}}$ versus reorganization energy λ and energy difference ΔE_0, as shown in Fig. 5C. On/off ratios smaller and larger than unity are obtained, depending on the precise parameter choice. Despite its simplicity, the model confirms that the experimentally observed on/off ratio of about an order of magnitude can be explained by the symmetry breaking induced by the aligned molecular dipoles. Moreover, it can accurately reproduce the magnitude and the field dependence of the on/off ratio, as shown in fig. S18.

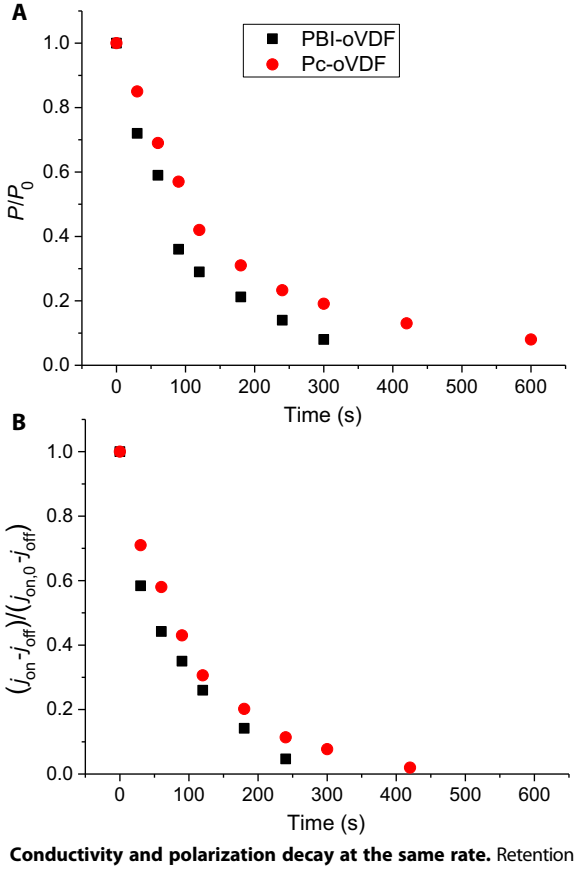

Fig. 4. Conductivity and polarization decay at the same rate. Retention of polarization (**A**) and current (**B**) in PBI-oVDF and Pc-oVDF oFESC diodes. Retention is measured by poling the diode and reading out the remaining polarization and the on-current after a waiting time *t*. During the waiting time, the device is grounded. Polarization and current measurements were taken successively on the same devices. *Y* axes are normalized to the values at $t = 0$ s; j_{off} is the current in the fully depolarized state. Other parameters are shown in Fig. 3.

CONCLUSION

In summary, we have designed and synthesized a new class of disc-like organic molecules that (i) are semiconducting, (ii) have dipolar side groups, and (iii) can be organized into columnar morphologies that have sufficient long-range order to support both ferroelectric coupling between the dipolar groups and quasi-1D charge transport. The ferroelectric polarization is shown to couple strongly to the materials' bulk conductivity, giving rise to switchable and rectifying current-voltage characteristics. The behavior is found for three distinct organic semiconductors that have two totally different dipolar side groups and can be explained quantitatively by a simple two-site model for hopping charge carriers. The observed phenomena are potentially relevant for low-cost nonvolatile rewritable memory applications and, in a broader perspective, demonstrate the possibility of modulating bulk material properties by ferroelectric polarization.

MATERIALS AND METHODS

Material synthesis

Details about the chemical synthesis and characterization of the materials can be found in section S1 and in studies of Guilleme *et al.* (*15*) and García-Iglesias *et al.* (*16*).

Device fabrication

Experimental metal/functional material/metal capacitor devices were fabricated in a typical cross-bar geometry on a glass substrate. All substrates were chemically cleaned and deionized. Top and bottom contacts were defined by high-vacuum ($\approx 2 \times 10^{-7}$ mbar) evaporation of 70-nm gold through a shadow mask; for a good adhesion, 5 nm of Cr was evaporated before deposition of the bottom electrode. The functional organic films were prepared by drop casting from a solution of dry materials (15 mg of SubPc and 20 mg of PBI-oVDF and Pc-oVDF) dissolved per 1 ml of chloroform. The resulting films had thicknesses of 1 to 4 μm, as checked by a Dektak profilometer. Film roughness was measured using atomic force microscopy, and root mean square values between 10 and 40 nm (5 μm × 5 μm scan) were found for ~1-μm-thick films. Typical device areas varied between 0.25 and 0.5 mm^2. Before deposition of the top contact, the cast films were thermally annealed at 85°C (SubPc) or 65°C (PBI-oVDF and Pc-oVDF). Before the ferroelectric measurements, films were aligned by applying a triangular wave voltage at elevated temperature, as described in section S2.

Electrical characterization

To reduce noise, the devices were electrically characterized inside a Janus probe station at atmospheric pressure. Switching signal waveforms were applied by an Agilent 33120A arbitrary waveform generator and amplified by a Falco WMA-300 high-voltage amplifier. The actual circuit current was measured by a Keithley 6485 picoammeter, which was visualized and stored on an Agilent DSO7104A oscilloscope for further analysis. To measure *jV* curves, a low-current Keithley 2636 SMU instrument was used. Measurement of a full *jV* curve (for example, from negative to positive back to negative bias) took typically several tens of seconds. With sweep rates that are substantially slower than those used for measuring polarization curves (see below), spurious currents due to polarization reversal (dP/dt) are suppressed, as also discussed in the main text [for the figures in the main text, 20 s (Fig. 2B, SubPc-amide), 40 s (Fig. 3B, PBI-oVDF), and 60 s (Fig. 3D, Pc-oVDF)].

Polarization-voltage (*P-V*) hysteresis loops, the characteristic curves of ferroelectrics, were obtained by integrating the pure switching-current response (dP/dt) as a difference between the full device response, which includes the relevant dP/dt signal and a subsequently measured background response that consists of only the leakage and displacement contributions. This way of achievement of remnant hysteresis loops at quasi-static conditions is known as the double-wave method (DWM) and is described by Fukunaga and Noda (*32*) and Khikhlovskyi *et al.* (*33*). Figure S9 briefly summarizes the DWM.

Model

The asymmetric charge transport, as observed in the experiments, is explained using a Marcus hopping model with an asymmetric potential. As for normal Marcus hopping, the energy barrier ΔE is determined by the intersection between the free energy parabolas of the initial and final sites, as shown in fig. S16A. Thus, the energy barrier is

$$\Delta E = \frac{\Delta z^2}{4\lambda}(\lambda + \Delta E_0)^2$$

where λ is the reorganization energy and Δz and ΔE_0 are the distance and energy difference between the two sites, respectively. The hopping

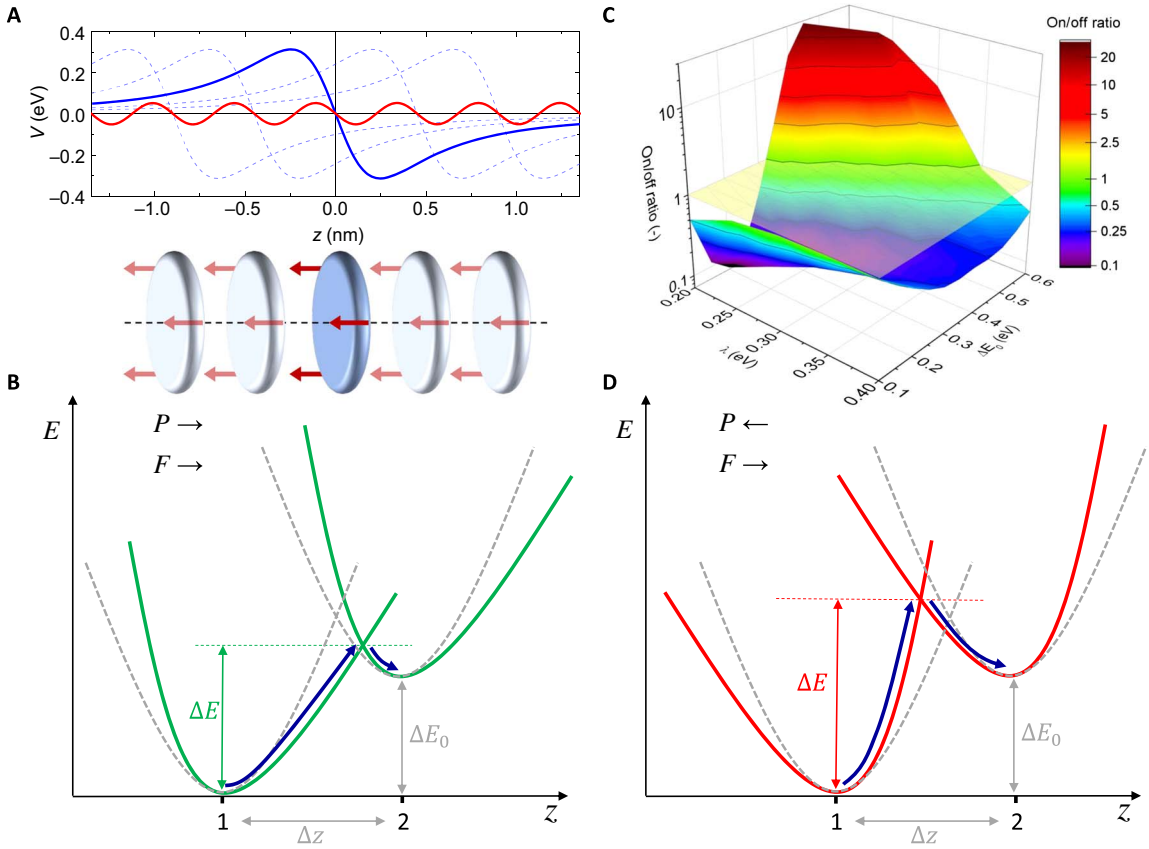

Fig. 5. Two-site model for bulk conductivity modulation based on Marcus hopping. (**A**) Electrostatic potentials of a single molecule (dark and light blue lines) and their sum (red line) of the stack of molecules shown in the lower half. The asymmetry of this potential energy landscape leads to a nonequivalence of hopping with the polarization *P* directed along (**B**) and against (**D**) the field *F*. Symmetric Marcus potentials are plotted as dashed curves in (B) and (D). The difference in energy barrier ΔE between the two polarization states causes a difference in conductivity at finite field. The resulting on/off ratio at a field of 100 V/μm is given in (**C**) as a function of reorganization energy λ and site energy difference ΔE_0.

rate ν is exponentially dependent on this energy barrier so that

$$\nu = \nu_0 \exp(\Delta E / k_B T)$$

where k_B is the Boltzmann constant and ν_0 is an attempt frequency.

The asymmetric potential as shown in Fig. 5A is added as a modulation onto the symmetric parabola. This results in a change in the energy barrier for hopping, and thus in the hopping rate, as shown schematically by the green line in fig. S16B.

To convert the (asymmetric) hopping rates into currents or mobilities, the simple two-site model with periodic boundary conditions in fig. S16C is considered. This model will not predict absolute currents, but it will be able to estimate the ratio of the currents for the two polarization directions. A charge carrier can hop from site 1 to site 2 and back, and do so either along or against the applied field, yielding four possible hops per polarization direction, as shown in fig. S16C.

The hopping rate is determined for each of these hops, and the mobility is thus calculated as a weighted ratio of the net hopping rate along the field and the total rate. This was done analytically and through a kinetic Monte Carlo technique, giving identical results. It is important to note that when the field approaches zero, the net current goes to zero. Simultaneously, the on/off ratio of currents (and mobilities) goes to one as required by symmetry. The parameters used for the calculation and a description of how they were obtained can be found in section S5.

SUPPLEMENTARY MATERIALS

Supplementary material for this article is available at http://advances.sciencemag.org/cgi/content/full/3/9/e1701017/DC1

section S1. Synthesis and material characterization
section S2. Device alignment and characterization
section S3. Detailed analysis of *jV* curves
section S4. *jV* curves on linear scale
section S5. Details of the two-site model
scheme S1. Synthetic method for the preparation of PBI-oVDF and Pc-oVDF.
scheme S2. Synthetic method for the preparation of SubPc-amide.
fig. S1. Structure of PBI-oVDF.
fig. S2. Characterization of PBI-oVDF.
fig. S3. Structure of Pc-oVDF.
fig. S4. Characterization of Pc-oVDF.
fig. S5. Structure of SubPc-amide.
fig. S6. NMR spectra of SubPc-amide.
fig. S7. Mass spectroscopy of SubPc-amide.
fig. S8. POM on SubPc.
fig. S9. Principle of the DWM.
fig. S10. Typical charging curves obtained by the DWM.
fig. S11. Analysis of a Pc-oVDF oFESC diode after incomplete field annealing.
fig. S12. Detailed analysis of current-voltage characteristics of oFESC diodes.
fig. S13. Hysteresis loop and current-voltage characteristics of PVDF-TrFE.
fig. S14. Same data as in Fig. 2B, plotted on linear scale.
fig. S15. Same data as in Fig. 3 (B and D), plotted on linear scale.
fig. S16. The potential landscape for hopping in the two-site model.
fig. S17. Geometry of the SubPc-amide molecule.
fig. S18. Experimental and simulated on/off ratio as a function of applied field.
table S1. Model parameters.
References (*34–41*)

REFERENCES AND NOTES

1. F. C. Grozema, L. D. A. Siebbeles, Mechanism of charge transport in self-organizing organic materials. *Int. Rev. Phys. Chem.* **27**, 87–138 (2008).
2. A. S. Tayi, A. K. Shveyd, A. C.-H. Sue, J. M. Szarko, B. S. Rolczynski, D. Cao, T. J. Kennedy, A. A. Sarjeant, C. L. Stern, W. F. Paxton, W. Wu, S. K. Dey, A. C. Fahrenbach, J. R. Guest, H. Mohseni, L. X. Chen, K. L. Wang, J. F. Stoddart, S. I. Stupp, Room-temperature ferroelectricity in supramolecular networks of charge-transfer complexes. *Nature* **488**, 485–489 (2012).
3. A. S. Tayi, A. Kaeser, M. Matsumoto, T. Aida, S. I. Stupp, Supramolecular ferroelectrics. *Nat. Chem.* **7**, 281–294 (2015).
4. A. V. Gorbunov, T. Putzeys, I. Urbanavičiūtė, R. A. J. Janssen, M. Wübbenhorst, R. P. Sijbesmad, M. Kemerink, True ferroelectric switching in thin films of trialkylbenzene-1,3, 5-tricarboxamide (BTA). *Phys. Chem. Chem. Phys.* **18**, 23663–23672 (2016).
5. V. Percec, M. Glodde, T. K. Bera, Y. Miura, I. Shiyanovskaya, K. D. Singer, V. S. K. Balagurusamy, P. A. Heiney, I. Schnell, A. Rapp, H.-W. Spiess, S. D. Hudson, H. Duan, Self-organization of supramolecular helical dendrimers into complex electronic materials. *Nature* **419**, 384–387 (2002).
6. D. Adam, P. Schuhmacher, J. Simmerer, L. Häussling, K. Siemensmeyer, K. H. Etzbachi, H. Ringsdorf, D. Haarer, Fast photoconduction in the highly ordered columnar phase of a discotic liquid crystal. *Nature* **371**, 141–143 (1994).
7. V. M. Fridkin, Bulk photovoltaic effect in noncentrosymmetric crystals. *Crystallogr. Rep.* **46**, 654–658 (2001).
8. K. Asadi, D. M. de Leeuw, B. de Boer, P. W. M. Blom, Organic non-volatile memories from ferroelectric phase-separated blends. *Nat. Mater.* **7**, 547–550 (2008).
9. K. Asadi, M. Li, P. W. M. Blom, M. Kemerink, D. M. de Leeuw, Organic ferroelectric opto-electronic memories. *Mater. Today* **14**, 592–599 (2011).
10. M. Kemerink, K. Asadi, P. W. M. Blom, D. M. de Leeuw, The operational mechanism of ferroelectric-driven organic resistive switches. *Org. Electron.* **13**, 147–152 (2012).
11. V. Khikhlovskyi, R. Wang, A. J. J. M. van Breemen, G. H. Gelinck, R. A. J. Janssen, M. Kemerink, Nanoscale organic ferroelectric resistive switches. *J. Phys. Chem. C* **118**, 3305–3312 (2014).
12. P. W. M. Blom, R. M. Wolf, J. F. M. Cillessen, M. P. C. M. Krijn, Ferroelectric Schottky diode. *Phys. Rev. Lett.* **73**, 2107–2110 (1994).
13. H. T. Yi, T. Choi, S. G. Choi, Y. S. Oh, S.-W. Cheong, Mechanism of the switchable photovoltaic effect in ferroelectric BiFeO3. *Adv. Mater.* **23**, 3403–3407 (2011).
14. A. V. Gorbunov, A. T. Haedler, T. Putzeys, R. H. Zha, H.-W. Schmidt, M. Kivala, I. Urbanavičiūtė, M. Wübbenhorst, E. W. Meijer, M. Kemerink, Switchable charge injection barrier in an organic supramolecular semiconductor. *ACS Appl. Mater. Interfaces* **8**, 15535–15542 (2016).
15. J. Guilleme, E. Cavero, T. Sierra, J. Ortega, C. L. Folcia, J. Etxebarria, T. Torres, D. González-Rodríguez, Polar switching in a lyotropic columnar nematic liquid crystal made of bowl-shaped molecules. *Adv. Mater.* **27**, 4280–4284 (2015).
16. M. García-Iglesias, B. F. M. de Waal, A. V. Gorbunov, A. R. A. Palmans, M. Kemerink, E. W. Meijer, A versatile method for the preparation of ferroelectric supramolecular materials via radical end-functionalization of vinylidene fluoride oligomers. *J. Am. Chem. Soc.* **138**, 6217–6223 (2016).
17. J. Guilleme, M. J. Mayoral, J. Calbo, J. Aragó, P. M. Viruela, E. Ortí, T. Torres, D. González-Rodríguez, Non-centrosymmetric homochiral supramolecular polymers of tetrahedral subphthalocyanine molecules. *Angew. Chem. Int. Ed.* **54**, 2543–2547 (2015).
18. C. F. C. Fitié, W. S. C. Roelofs, M. Kemerink, R. P. Sijbesma, Remnant polarization in thin films from a columnar liquid crystal. *J. Am. Chem. Soc.* **132**, 6892–6893 (2010).
19. C. F. C. Fitié, W. S. C. Roelofs, P. C. M. M. Magusin, M. Wübbenhorst, M. Kemerink, R. P. Sijbesma, Polar switching in trialkylbenzene-1,3,5-tricarboxamides. *J. Phys. Chem. B* **116**, 3928–3937 (2012).
20. D. Miyajima, F. Araoka, H. Takezoe, J. Kim, K. Kato, M. Takata, T. Aida, Ferroelectric columnar liquid crystal featuring confined polar groups within core–shell architecture. *Science* **336**, 209–213 (2012).
21. T. Choi, S. Lee, Y. J. Choi, V. Kiryukhin, S.-W. Cheong, Switchable ferroelectric diode and photovoltaic effect in $BiFeO_3$. *Science* **324**, 63–66 (2009).
22. R. Waser, M. Aono, Nanoionics-based resistive switching memories. *Nat. Mater.* **6**, 833–840 (2007).
23. K. M. Kim, D. S. Jeong, C. S. Hwang, Nanofilamentary resistive switching in binary oxide system; a review on the present status and outlook. *Nanotechnology* **22**, 254002 (2011).
24. M. Lanza, A review on resistive switching in high-k dielectrics: A nanoscale point of view using conductive atomic force microscope. *Materials* **7**, 2155–2182 (2014).
25. D. S. Jeong, R. Thomas, R. S. Katiyar, J. F. Scott, H. Kohlstedt, A. Petraru, C. S. Hwang, Emerging memories: Resistive switching mechanisms and current status. *Rep. Prog. Phys.* **75**, 076502 (2012).
26. I. Urbanaviciute, X. Meng, T. D. Cornelissen, A. V. Gorbunov, S. Bhattacharjee, R. P. Sijbesma, M. Kemerink, Tuning the ferroelectric properties of trialkylbenzene-1,3, 5-tricarboxamide (BTA). *Adv. Electron. Mater.* **3**, 1600530, (2017).
27. A. V. Gorbunov, X. Meng, I. Urbanaviciute, T. Putzeys, M. Wübbenhorst, R. P. Sijbesma, M. Kemerink, Polarization loss in the organic ferroelectric trialkylbenzene-1,3,5-tricarboxamide (BTA). *Phys. Chem. Chem. Phys.* **19**, 3192–3200 (2017).
28. D. B. Strukov, G. S. Snider, D. R. Stewart, R. S. Williams, The missing memristor found. *Nature* **453**, 80–83 (2008).
29. S. van Reenen, P. Matyba, A. Dzwilewski, R. A. J. Janssen, L. Edman, M. Kemerink, A unifying model for the operation of light-emitting electrochemical cells. *J. Am. Chem. Soc.* **132**, 13776–13781 (2010).
30. J. C. Scott, L. D. Bozano, Nonvolatile memory elements based on organic materials. *Adv. Mater.* **19**, 1452–1463 (2007).
31. M.-J. Lee, C. B. Lee, D. Lee, S. R. Lee, M. Chang, J. H. Hur, Y.-B. Kim, C.-J. Kim, D. H. Seo, S. Seo, U.-I. Chung, I.-K. Yoo, K. Kim, A fast, high-endurance and scalable non-volatile memory device made from asymmetric Ta_2O_{5-x}/TaO_{2-x} bilayer structures. *Nat. Mater.* **10**, 625–630 (2011).
32. M. Fukunaga, Y. Noda, New technique for measuring ferroelectric and antiferroelectric hysteresis loops. *J. Phys. Soc. Jpn.* **77**, 064706 (2008).
33. V. Khikhlovskyi, A. V. Gorbunov, A. J. J. M. van Breemen, R. A. J. Janssen, G. H. Gelinck, M. Kemerink, Multi-bit organic ferroelectric memory. *Org. Electron.* **14**, 3399–3405 (2013).
34. D. Hong, M. Lv, M. Lei, Y. Chen, P. Lu, Y. Wang, J. Zhu, H. Wang, M. Gao, S. E. Watkins, X. Chen, *N*-acyldithieno[3,2-*b*:2′,3′-*d*]pyrrole-based low-band-gap conjugated polymer solar cells with amine-modified [6,6]-phenyl-C61-butyric acid ester cathode interlayers. *ACS Appl. Mater. Interfaces* **5**, 10995–11003 (2013).
35. J. Guilleme, J. Aragó, E. Ortí, E. Cavero, T. Sierra, J. Ortega, C. L. Folcia, J. Etxebarria, D. González-Rodríguez, T. Torres, A columnar liquid crystal with permanent polar order. *J. Mater. Chem. C* **3**, 985–989 (2015).
36. R. Pandey, A. A. Gunawan, K. A. Mkhoyan, R. J. Holmes, Efficient organic photovoltaic cells based on nanocrystalline mixtures of boron subphthalocyanine chloride and C_{60}. *Adv. Funct. Mater.* **22**, 617–624 (2012).
37. R. Agrawal, P. Kumar, S. Ghosh, A. K. Mahapatro, Thickness dependence of space charge limited current and injection limited current in organic molecular semiconductors. *Appl. Phys. Lett.* **93**, 073311 (2008).
38. C. G. Claessens, U. Hahn, T. Torres, Phthalocyanines: From outstanding electronic properties to emerging applications. *Chem. Rec.* **8**, 75–97 (2008).
39. V. R. Ferro, J. M. García de la Vega, R. H. González-Jonte, L. A. Poveda, A theoretical study of subphthalocyanine and its nitro- and *tert*butyl-derivatives. *J. Mol. Struct. THEOCHEM* **537**, 223–234 (2001).
40. N. Kobayashi, T. Ishizaki, K. Ishii, H. Konami, Synthesis, spectroscopy, and molecular orbital calculations of subazaporphyrins, subphthalocyanines, subnaphthalocyanines, and compounds derived therefrom by ring expansion. *J. Am. Chem. Soc.* **121**, 9096–9110 (1999).
41. R. A. Kipp, J. A. Simon, M. Beggs, H. E. Ensley, R. H. Schmehl, Photophysical and photochemical investigation of a dodecafluorosubphthalocyanine derivative. *J. Phys. Chem. A* **102**, 5659–5664 (1998).

Acknowledgments: We are grateful to R. P. Sijbesma, R. A. J. Janssen, and P. A. Bobbert for stimulating discussions. **Funding:** The work of A.V.G. was supported by the Netherlands Organization for Scientific Research (NWO) Nano program. The work of J.G. was funded by the Ministerio de Educación, Culture y Deporte (MECD) (FPU fellowship). This work was supported by MINECO, Spain (grants CTQ-2014-52869-P to T.T. and CTQ2014-57729-P to D.G.-R.), Comunidad de Madrid (grant S2013/MIT-2841 FOTOCARBON to T.T.), and the European Research Council (grant StG-279548 to D.G.-R.). The Dutch Polymer Institute is thanked for funding M.G.I. and the Dutch Ministry of Education, Culture and Science (Gravitation program 024.001.035) for funding E.W.M. T.D.C. acknowledges financial support from the Swedish Government Strategic Research Area in Materials Science on Functional Materials at Linköping University (Faculty Grant SFO-Mat-LiU no. 2009 00971). **Author contributions:** A.V.G. and W.S.C.R. performed the ferroelectric experiments. M.G.I. and J.G. synthesized and characterized materials. T.T., D.G.-R., E.W.M., and M.K. coordinated research. T.D.C. and M.K. developed the theoretical model. M.K. and E.W.M. wrote the manuscript. All authors contributed to and commented on the manuscript. **Competing interests:** The authors declare that they have no competing interests. **Data and materials availability:** All data needed to evaluate the conclusions in the paper are present in the paper and/or the Supplementary Materials. Additional data related to this paper may be requested from the authors.

Submitted 28 March 2017
Accepted 6 September 2017
Published 29 September 2017
10.1126/sciadv.1701017

Citation: A. V. Gorbunov, M. Garcia Iglesias, J. Guilleme, T. D. Cornelissen, W. S. C. Roelofs, T. Torres, D. González-Rodríguez, E. W. Meijer, M. Kemerink, Ferroelectric self-assembled molecular materials showing both rectifying and switchable conductivity. *Sci. Adv.* **3**, e1701017 (2017).